

# Analysis of Wing Morphing via Frame Buckling

A. Srikantha Phani<sup>1</sup>, Richard Butler<sup>2</sup>, Stephen Habgood<sup>3</sup>  
and Christopher R. Bowen<sup>4</sup>  
*University of Bath, Bath, BA2 7AY, UK*

This paper presents structural analysis methods to model morphing, achieved via buckling of struts in multi-element structural components. An exact element theory and an energy-based variational approach are used to deduce a closed-form relationship between actuator force and displacement, by firstly assuming an ideal actuator. Subsequently, the flexibility of the actuator is incorporated via a lumped parameter model to account for actuator-structure interaction. The single element actuation concept is extended to multi-element frame architecture to produce displacements of an example aircraft tail section, by actuating one or two elements of the assembly. Hybrid actuation, combining large force with large displacement actuators is also introduced, whereby large shape changes can be achieved with optimum demand on the actuators. It is concluded that exact element theory has significant potential in deducing closed-form relationship between the actuator forces and structural displacements. The energy approach, based on the trial function to represent the displacements, is shown to be approximate, but sufficient. These closed-form relationships can be readily used in optimisation routines to achieve an optimal structure to produce structural shape changes.

## Nomenclature

$\alpha$	=	Sway displacement
$\varepsilon$	=	End-shortening of a strut
$\delta$	=	Displacement of the structure along the actuator axis
$P_E$	=	Euler critical load of a strut
$F$	=	Force in the actuator
$F_b$	=	Blocking-force of the actuator
$\delta_f$	=	Free displacement of the actuator
$K_s$	=	Equivalent spring constant of the structure
		All other terms are defined within the text

## I. Introduction

STRUCTURAL morphing, or shape control, of aerodynamic components can potentially offer significant improvements in performance, for example, by altering wing shape to reduce drag during the various stages of cruise. The trailing edge geometry of an aerofoil section, both in terms of “boat tail angle” and cambering has an extremely powerful effect on the pressure distribution and hence the lift and drag of a wing. It controls not only the local load at the rear but also the circulation around the aerofoil and thereby the lift generated along the complete chord. As well as obvious applications to controllability, relatively small changes, even of just a few degrees applied over the last few percent of the wing chord, can have a significant effect on the cruise characteristics of the wing. This is the well known “Variable Camber” technique which can be used to tune the wing section characteristics differentially across the wing span at different flight conditions, and hence be used to reduce drag and/or wing loads (weight) to reduce fuel burn and emissions.

A variety of approaches have been investigated to achieve shape change in structures. These range from the use of compliant mechanisms<sup>1</sup> to bi-stable concepts that exhibit some form of snap-through behaviour, occurring for

---

<sup>1</sup> University Research Fellow, Department of Mechanical Engineering, e-mail: spa21@bath.ac.uk.

<sup>2</sup> Senior Lecturer, Department of Mechanical Engineering, e-mail: R.Butler@bath.ac.uk.

<sup>3</sup> Undergraduate Student, Department of Mechanical Engineering, e-mail: en3sh@bath.ac.uk.

<sup>4</sup> Reader, Department of Mechanical Engineering, e-mail: C.R.Bowen@bath.ac.uk.

example, within trusses<sup>2</sup> or un-symmetric composite laminates<sup>3</sup>. One tried and tested method of inducing shape change is by the use of piezoelectric materials, which are able to generate high forces (of the order of kN), although the developed strains tend to be small, typically only 0.1 – 0.4%. However, such strain can be used to introduce bending or buckling into a structure to generate useful deflections.

Post-buckling of single strut components has also been successfully used to magnify the performance of piezoelectric actuators used to control a UAV with morphing wing<sup>4</sup> and to enable optimized variable camber aerofoil design<sup>5</sup>. Buckling of structural members leads to a reduction in their structural stiffness, hence, a reduction in the demand on the actuator force to induce a given displacement. Bi-stability provides another alternative approach to achieve a “softer” host structure against which actuators have to work to produce a shape change. An optimal combination of these concepts might be fruitful in practice.

The objective of the present study is to consider morphing of single-element and multi-element skeletal structures with embedded actuators to achieve shape change. A multi-element structure could represent a trailing edge rib of an aircraft wing, while a single element could represent a rib or spar of the wing of a micro aero vehicle. Exact element theory and an approximate energy minimisation technique are preferred over the conventional finite element analysis (FEA) to deduce closed form relationships. The paper is structured as follows. Morphing concepts based on buckling are introduced in Section II. An exact element methodology and an approximate energy based method are employed in Section III to deduce the relationship between the actuator force and the displacements, assuming an ideal actuator. The actuator-structure interaction is considered in Section IV, and lumped parameter models are presented. The importance of nonlinearities in structural stiffness is highlighted. Hybrid actuation concepts, employing two actuators to achieve large forces as well as large displacements, are introduced and analysed in Section V. Main conclusions from this study are summarised in Section VI.

## II. Morphing Concepts

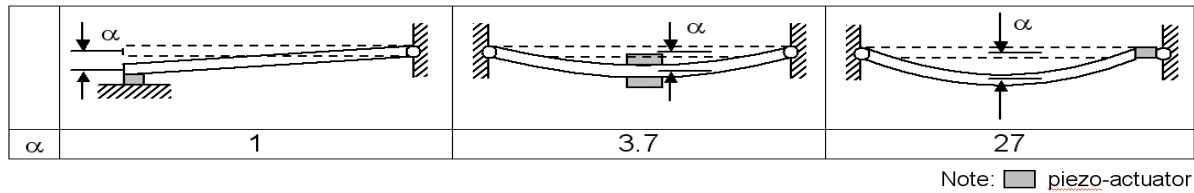


**Figure 1. Comparison of amplitude for piezo-actuation of, respectively, a linear actuator (left), a composite beam (middle) and a composite strut (right). In each case, the same beam dimensions were used, and an equal electric field was applied over an equivalent device length. A value of  $(\epsilon - \epsilon^c)/L$  of approximately 0.05% was applied.**

The actuation of a simply supported single beam/strut has been studied earlier by the authors to determine the capability of piezoelectric actuation for aero-structural morphing. In the first approach, a piezoelectric composite patch was bonded to the surface of a composite beam, and in the second, a piezoelectric stack was placed at the end of a strut to produce buckling. These previous studies showed that more than seven times greater amplification was possible when using the buckled strut and stack to achieve out-of-plane displacement, compared with actuation via the patch, see Fig. 1. This is because the compressive displacement  $\epsilon$  provided by the stack is amplified according to the well-known geometric relationship for sinusoidal deflection

$$\frac{\alpha}{L} = \frac{2}{\pi} \sqrt{\frac{(\epsilon - \epsilon^c)}{L}} \quad (1)$$

where  $L$  is the original length of the strut,  $\alpha$  is the amplitude of the buckled strut arising from the difference between total end shortening,  $\epsilon$ , following buckling and the end displacement required to buckle the strut,  $\epsilon^c$ . Clearly, the enhanced amplitude  $\alpha$  is possible only in the vicinity of buckling, where the structure loses its initial stiffness. This also suggests that buckling can be effectively used to morph multi-element structural assemblies by actuating one or more members of the assembly. In the sequel, morphing via buckling of struts will be considered in detail.

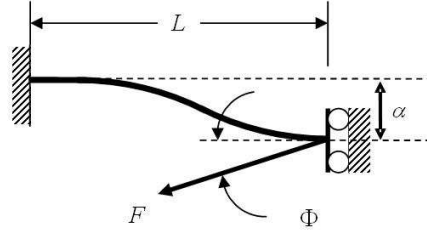


Figure 2. Sway member with actuator force  $F$  inclined at  $\Phi$  to horizontal

### III. Structural Analysis

#### A. Single Strut

The analysis presented in this section can be applied to both a single element and multi-element actuation configurations. Consider, first, a single strut subjected to an actuation, the actuator force and boundary conditions are shown in Fig. 2.

Moment equilibrium about a cut along the member at B, in Fig. 3, gives

$$M = -EI \frac{d^2 w}{dx^2} = Pw + m_1 - P_{z1}x \quad \text{where, } P_{z1} = -F \sin(\Phi) \text{ and } P = F \cos(\Phi) \quad (2)$$

and  $E$  is the elastic modulus,  $I$  is the second moment of area of the beam and  $P_{z1}$  and  $m_1$  define the force in the  $z$ -direction and moment at the end, respectively. This has a general solution

$$w(x) = C_1 \cos(\beta x) + C_2 \sin(\beta x) - \frac{m_1}{P} + \frac{P_{z1}x}{P}, \quad \beta^2 \equiv \frac{P}{EI} \quad (3)$$

in which  $C_1$  and  $C_2$  are unknown coefficients found through application of the particular boundary conditions. The boundary conditions relevant to the strut model shown in Fig. 2 are

$$w(0) = 0, \quad \left[ \frac{dw}{dx} \right]_{x=0} = 0, \quad w(L) = \alpha, \quad \left[ \frac{dw}{dx} \right]_{x=L} = 0 \quad (4)$$

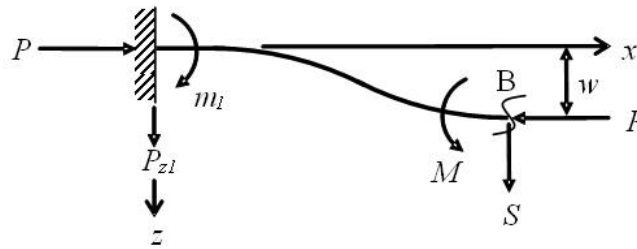


Figure 3. Forces and displacements for a general post-buckled member.

Solution of Eqn. (2) for boundary conditions in Eqn. (4) gives rise to stability functions<sup>7</sup>. Such analytical methods have the ability to pin-point the initial buckling load, and trace the buckling path more accurately than FEA methods. Since they only require one element per member, they are ideally suited to iterative design methods, and provide deeper insight than can be obtained from large FEA models. Hence we employ stability functions for this analysis. The displacement solution  $w$  for the boundary conditions given in Eqn. (4) is:

$$w(x) = \frac{-P_{z1}}{P\beta} [(\cos ec(\beta L) - \cot(\beta L))(\cos(\beta x) - 1) + \beta x - \sin(\beta x)]. \quad (5)$$

Using Eqn. (5) the sway displacement  $\alpha$  is given by:

$$\alpha \equiv w(x=L) = \frac{-P_{z1}L^3}{EI} \frac{m}{2s(1+c)} \quad (6)$$

where the stability functions  $m$ ,  $s$  and  $c$  are defined below

$$m = \frac{\tan(\gamma)}{\gamma}, \quad s = \frac{\gamma(1-2\gamma \cot(2\gamma))}{\tan(\gamma)-\gamma}, \quad c = \frac{(2\gamma - \sin(2\gamma))}{\sin(2\gamma)(1-2\gamma \cot(2\gamma))}, \quad \gamma \equiv \frac{\pi}{2} \sqrt{\frac{P}{P_E}}, \quad P_E \equiv \frac{\pi^2 EI}{L^2}. \quad (7)$$

The flexural end-shortening can be obtained from  $w(x)$  via

$$\varepsilon = \frac{1}{2} \int_{x=0}^L \left[ \frac{dw}{dx} \right]^2 dx \quad (8)$$

The net displacement along the actuator is given in terms of  $\alpha$  and  $\varepsilon$  by a suitable co-ordinate transformation from strut-axes to actuator axes as follows:

$$\delta = \alpha \sin(\Phi) + \varepsilon \cos(\Phi) \quad (9)$$

An alternative to the exact element theory to obtain approximate closed-form expressions for  $\alpha$  and  $\varepsilon$  is via a Rayleigh-Ritz based energy approach. In this approach one minimises the total potential energy of the strut in Fig. 3 given by

$$V = \frac{1}{2} \int_0^L EI \left( \frac{d^2 w}{dx^2} \right)^2 dx - F \sin(\Phi) \alpha - F \cos(\Phi) \varepsilon \quad (10)$$

Assuming a suitable trial function for the displacement field  $w(x)$  parameterised by  $\alpha$  of the form

$$w(x) = \frac{\alpha}{2} \left[ 1 - \cos\left(\frac{\pi x}{L}\right) \right], \quad (11)$$

the total potential energy of the system in Eqn. (10) can be written in terms of  $\alpha$  as the unknown. Noting that stable equilibrium is a minimum energy configuration, a constraint equation on  $\alpha$  is obtained as

$$\frac{dV}{d\alpha} = 0, \quad (12)$$

which gives a closed-form expression for  $\alpha$ :

$$\frac{\alpha}{L} = \frac{8 \frac{F}{P_E} \sin(\Phi)}{\pi^2 \left( 1 - \frac{F}{P_E} \cos(\Phi) \right)} \quad (13)$$

A similar approach can be followed for  $\varepsilon$ , which leads to

$$\frac{\varepsilon}{L} = \left[ \frac{2 \frac{F}{P_E} \sin(\Phi)}{\pi \left( 1 - \frac{F}{P_E} \cos(\Phi) \right)} \right]^2 = \frac{\pi^2}{16} \left[ \frac{\alpha}{L} \right]^2. \quad (14)$$

It is noteworthy that comparison of Eqns. (1) and (14) reveal that the sway displacement achievable using the strut arrangement in Fig. 2 is double the maximum amplitude obtained for a similar, pin-ended strut with equivalent end-shortening (Fig. 1).

Comparison between the exact element theory and the approximate energy method is made by computing  $\alpha$  and  $\varepsilon$  for a low, and a high value of the actuator inclination  $\Phi$ . The results in Fig. 4 suggest that the expressions in Eqns. (13) and (14) are sufficient for the purposes of engineering analysis. A similar degree of accuracy is noted between the  $\delta$  values (not shown).

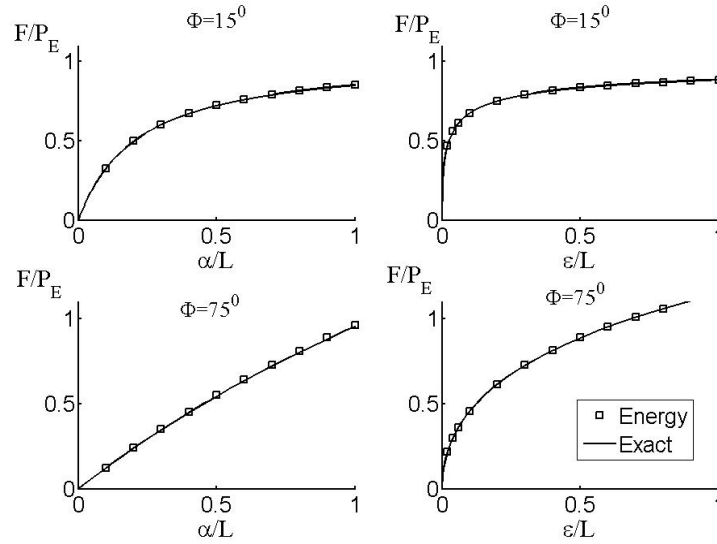
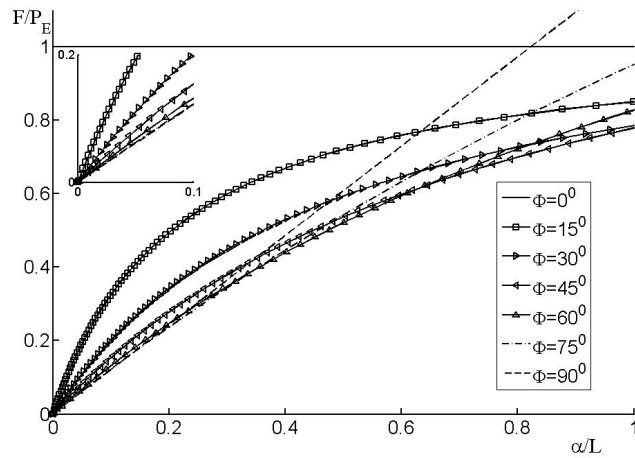
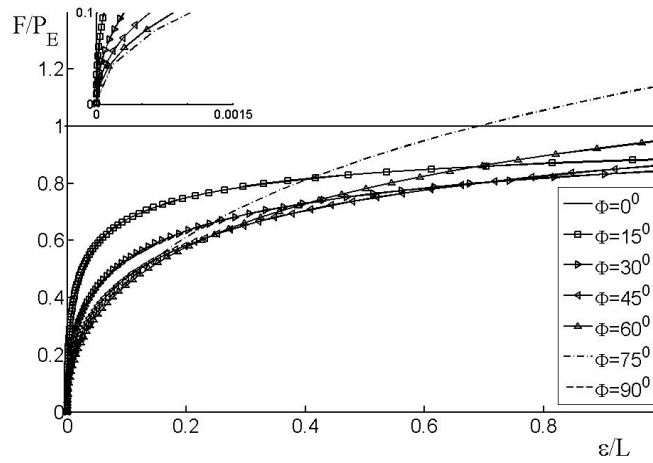


**Figure 4. Comparison of sway  $\alpha$  and end shortening  $\varepsilon$  displacements predicted by the exact element theory (solid line) and the approximate energy expression (square points) in Eqns. (13) and (14).**

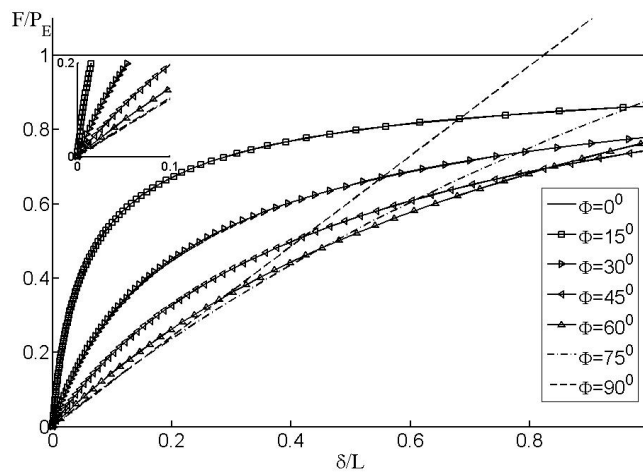
For the strut of Fig. 2, stability functions have been used to give the plot of actuator force  $F$  against sway displacement  $\alpha$ , for various values of actuator inclination angle  $\Phi$ . The dependence of end-shortening  $\varepsilon$ , and total displacement  $\delta$  along the actuator direction, upon the actuator force were also computed and plotted in Fig. 5. Consider the  $F$  Vs.  $\alpha$  plot, first. When the force is applied axially ( $\Phi = 0^\circ$ ) the standard bifurcation plot (horizontal solid line in Fig. 5(a)) is obtained whereby no lateral displacement is produced before the buckling load  $P_E$ , at which  $\alpha$  becomes infinite. For the case when the actuator force is entirely lateral ( $\Phi = 90^\circ$ ) the member behaves as a beam with linear stiffness ( $12EI/L^3$ ) (dashed line in Fig. 5(a)). For intermediate values of  $\Phi$  between  $0^\circ$  and  $90^\circ$ , the associated curves are asymptotic to buckling loads at  $F/P_E = \sec(\Phi)$ . Consequently, high values of  $\Phi$  are better at achieving displacement control for low  $F$ . Low values of  $\Phi$  are better at higher values of  $F$ . A similar dependence of the end-shortening  $\varepsilon$  on the actuator force  $F$  can be observed in Fig. 5(b). The net displacement  $\delta$  oriented along the actuator also shows similar dependence on  $\Phi$ , see Fig. 5 (c).



(a) Force Vs. Sway



(b) Force Vs. End-shortening



(c) Force Vs. Displacement of the actuator

**Figure 5. Actuator force  $F$ , normalized with respect to Euler load,  $\pi^2 EI/L^2$ , against displacements, normalized with respect to member length  $L$ , for sway member shown in Fig. 2 with varying actuator inclination  $\Phi$ . The inset in each diagram shows a magnified view closer to the origin.**

Initial imperfections in a single strut can be easily accommodated by modifying Eqn. (2), and repeating the analysis. When an imperfection of the form

$$w_0 = \frac{\alpha_0}{2} \left[ 1 - \cos\left(\frac{\pi x}{L}\right) \right] \quad (15)$$

in the bifurcation mode is assumed, Eqn. (2) becomes

$$M = -EI \frac{d^2 w}{dx^2} = P[w + w_0] + m_1 - P_{z1} x \quad (16)$$

which gives additional displacement according to the sign of  $\alpha_0$ .

The above analysis for sway and end-shortening of the single strut model can be useful in a multi-element structural frame assembly, which will now be discussed.

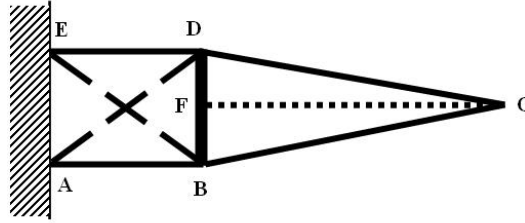


**Figure 6. An idealized 5-element trailing edge framework for wing morphing. The member  $BD$  has considerably high flexural rigidity  $EI$  compared to the rest, such that a pure sway of the frame  $ABDE$  is possible. The actuators are shown as dashed lines. The dotted line  $FC$  is a post-buckled pre-compressed member.**

## B. Multi-element structures

The requirements for morphing, in the context of the trailing edge, are to achieve a translation (sway), and a rotation/tilt (bending) displacement. This can be accomplished via a multi-element skeletal frame assembly sketched in Fig. 6. It is possible to induce pure sway, or pure rotation, through careful structural design of the frame. For example, pure sway can be accomplished by increasing the flexural rigidity of the member  $BD$  in Fig. 6. In practice, however, both sway and rotation have to be induced on the same structure. The sway displacements can be produced by using a hybrid system comprising of piezoelectric stacks to induce buckling in the struts  $AB$  and  $DE$  shown in the figure, and conventional actuators within inclined bracing elements (shown as dashed lines in Fig. 6) to control displacements. Rotational displacements have to be imposed upon the swayed frame. This can be achieved in three ways: a) bending the individual struts  $BC$  and  $CD$  using piezo-bimorph benders, b) introducing a post-buckled pre-compressed element  $FC$  (shown as a dotted line in Fig. 6) as introduced in Ref. 4, or c) differential end-shortening of the two struts  $AB$  and  $DE$ . In the last case, the members  $BC$  and  $CD$  are assumed to be rigid links, pinned to the frame  $ABDE$  at the joints  $B$  and  $D$ . The location of point  $C$  in the morphed state is purely governed by the kinematic requirement that the lengths of  $BC$  and  $CD$  are preserved.

The load carrying capacity, or stiffness, of the morphed structure depends on the degree of “redundancy” present in the initial un-morphed structure<sup>8-10</sup>. A *simply stiff* skeletal frame, obeying the Maxwell-Calladine rule<sup>8,9</sup>, is ideal in this regard, as it not only offers less resistance to a change in shape but can also carry loads in the morphed state. Here a *simply stiff* structure denotes a structure with no static and kinematic indeterminacies. Notice that a pin-jointed equivalent truss of the frame  $ABCDE$  in Fig. 6 has a four-bar like linkage whereby the frame  $ABDE$  has a shear mechanism. Hence the frame is not a *simply stiff* structure. However, if the presence of one actuator along the diagonal  $AD$  or  $BE$  is included, then the equivalent truss is *simply stiff*. Two independent actuators along  $AD$  and  $BE$  would result in a statically redundant equivalent truss, giving more stiffness in the morphed state, but, such an arrangement is also more difficult to morph.

Consider the frame  $ABCDE$  with actuators connected to members  $AB$  and, or  $DE$ . For the purposes of sway analysis one can envisage the sub-frame  $ABDE$  within the main frame  $ABCDE$ , comprising two parallel springs  $AB$

and  $DE$ . If the two members  $AB$  and  $DE$  are identical, then it is sufficient to analyse only one member  $AB$ , with a single inclined actuator  $EB$ . Thus the sway displacement  $\alpha$  normal to  $AB$ , end-shortening  $\varepsilon$  along  $AB$ , and the net displacement along the actuator  $\delta$  vary as shown in Fig. 5 for different actuator inclinations.

When the two members  $AB$  and  $DE$  are not identical, one would expect differential end-shortening  $\Delta\varepsilon$  leading to a tilt, or in-plane rotation, of the rigid horizontal member  $BD$ . The magnitude of this tilt is equal to  $\Delta\varepsilon/l$ , where  $l$  is the length of the member  $BD$ . Thus the frame  $BCD$  would rotate relative to the frame  $ABDE$ . Kinematic requirement of rigid bars  $BC$  and  $CD$  would govern the location of the tip  $C$  in the tilted configuration. Note that the amount of tilt achieved via differential end-shortening can be controlled, passively, by varying the length  $l$  of  $BD$  according to the lever-arm principle, or actively by changing  $\Delta\varepsilon$ . Note that the end-shortening  $\varepsilon$  is much smaller compared to sway displacement  $\alpha$  (see Eqn. (14)), suggesting that shorter lengths of  $BD$  are ideal.

The sway displacement of the frame can be increased by introducing an imperfection in the form of the first critical mode, in principle. For example, a larger differential end shortening, and hence rotation, could be achieved by applying tensile load to an initially curved strut  $AB$  whilst applying compression to the strut  $DE$ .

#### IV. Actuation Stiffness

Thus far, the actuator-structure interaction is ignored. The important actuator characteristics relevant to structural morphing application are blocking-force and free-displacement. Blocking-force  $F_b$  is the maximum force an actuator can develop when it is reacting against a fixed constraint. Free-displacement  $\delta_f$  is the maximum displacement an actuator can develop when there is no restraint against it. Whilst hydraulic actuators can develop large displacements  $\delta_f$  they have low blocking-force  $F_b$ . Piezoelectric stack actuators can develop large forces but cannot induce large displacements. The *actual* force and displacement developed by an actuator *in-situ* depends on the characteristics of the host structure. This interaction is considered here in detail, using simple models.

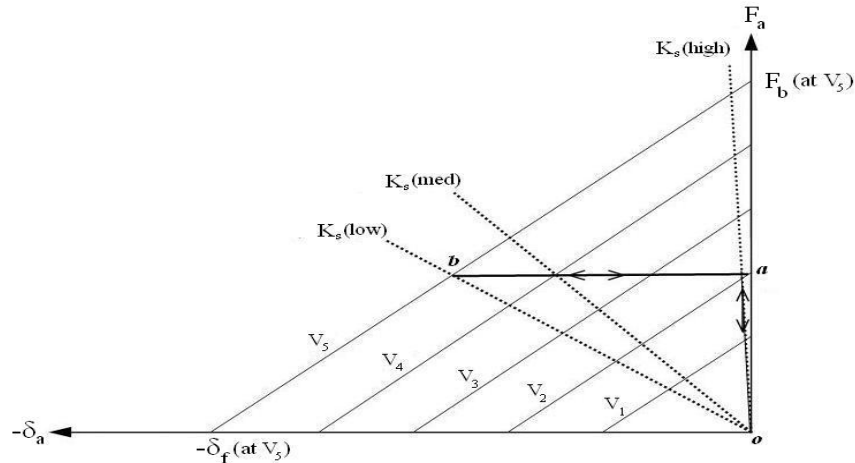


**Figure 7. Working diagram of an actuator working against a spring. Hard springs  $K_s(\text{high})$  lead to more force development in the actuator, and softer springs  $K_s(\text{low})$  result in more displacement.  $F_b$  is blocking-force;  $\delta_f$  free displacement;  $K_a$  actuator stiffness;  $F_a$  actuator force;  $\delta_a$  actuator displacement;  $V_1$  to  $V_5$  are the increasing magnitudes of the voltages supplied to the piezo actuator. Note that the negative displacement indicates that the piezo actuator is shortening.**

Consider, for example, a piezoelectric stack actuator working compressively against a spring of constant stiffness  $K_s$ . The working diagram is illustrated in Fig. 7. The force developed in the actuator  $F_a$  to produce a displacement  $\delta_a$  is given in terms of the blocking-force  $F_b$  and actuator stiffness  $K_a$  by

$$F_a = F_b + K_a \delta_a. \quad (17)$$

Note that the blocking-force and free-displacements depend on the operating voltage. The spring also extends/contracts by an amount equal to the actuator displacement  $\delta_s = \delta_a$  to ensure kinematic compatibility. Given the relationship in Eqn. (17), the actuator displacement  $\delta_a = \delta_s$  is given by:

$$\delta_a = \delta_s = \delta_f \left[ 1 - \frac{F_a}{F_b} \right], \quad (18)$$

or alternatively,

$$F_a = F_b \left[ 1 - \frac{\delta_a}{\delta_f} \right]. \quad (19)$$

Given that the spring force is equal and opposite to the force exerted by the piezo actuator  $F_a$ , force equilibrium condition  $F_a - F_s = 0$  together with Eqn. (19) and Eqn. (18) gives:

$$F_s = K_s \delta_s = F_a = F_b \left[ 1 - \frac{\delta_a}{\delta_f} \right], \quad (20)$$

which can also be expressed as

$$\delta_s = \frac{F_b}{K_a + K_s}. \quad (21)$$

The above relationship agrees with the intuitive deduction that, for a given actuator, that is with a specified  $K_a$ , a softer spring deforms more than a stiffer spring. The analysis so far has been centered around a simple *linear* spring.

Returning now to the sway frame in Fig. 6, one can envisage a simple model for the actuator-structure interaction, whereby the member  $AB$  of the frame is equated to a spring against which the actuator works. One can also immediately deduce that the spring is *nonlinear* in our case: the force displacement characteristics of interest are the  $F$  vs.  $\delta$  curves displayed in Fig. 5, for each inclination of the actuator. Thus, the exact element analysis can be successfully coupled with actuator characteristics via Eqn. (21) to account for the actuator-structure interaction.

## V. Hybrid Actuation

The analysis in Section III suggests that if the axial load component is close to buckling then very little additional sway force is necessary to generate large displacements values of  $\alpha$ ,  $\varepsilon$ , and  $\delta$ . For this reason, the optimum may be a hybrid actuation system, in which axial load is applied via a piezoelectric stack with low inclination  $\Phi$ , and sway control is subsequently achieved using a large displacement actuator, such as a hydraulic actuator, at high inclination  $\Phi$ . This would require the piezoelectric actuator to supply a constant force in the regime where the hydraulic actuator is producing large displacements.

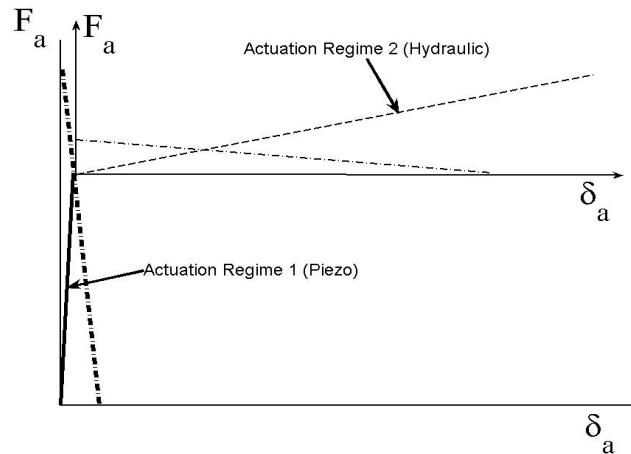


**Figure 8. Hybrid actuation. In the actuation Regime 1, a piezo actuator loads the strut initially, and then a hydraulic actuator switches on to induce large displacement in actuation Regime 2. The piezo actuator force in Regime 2 is ideally held at a constant value and the actuator behaves like a yielding spring.**

For a piezoelectric actuator, the force it can potentially deliver is not constant over its range of motion<sup>11</sup>, whereas hydraulic actuators can deliver a low, but constant force, over a relatively large displacement. The force available from a piezoelectric actuator progressively decreases as it extends and it is therefore important to consider the stiffness of the actuator  $K_a$  and the stiffness of the structure  $K_s$  it is acting against, as described in Section IV. The free-displacement  $\delta_f$  is typically 0.1% strain for multi-layer piezoelectric actuators<sup>12</sup>.

The working diagram for the proposed hybrid system is illustrated in Fig. 8, and Fig. 7 shows the characteristics of the piezo actuator. It is assumed that both free deflection and blocking-force are proportional to actuator voltage and actuator stiffness is independent of voltage; although piezoelectric materials can exhibit a range of nonlinearities, particularly at high electric fields where extrinsic effects due to domain wall motion can influence strain and stiffness<sup>13</sup>. To apply a constant load, as the hydraulic actuator displaces the structure, the piezoelectric actuator must be able to maintain a constant force with actuator deflection. This could be achieved, for example, by following path  $ab$  in Fig. 7 where the voltage is increased in magnitude from  $V_2$  to  $V_5$ . Delivery of a constant force requires the structure stiffness  $K_s$  to decrease as the actuation displacement increases. In effect, as the structure is loaded from point  $o$  in Fig. 7 whereupon it follows the path  $oab$ , along the initial stiffness line  $oa$ , and then along the zero effective stiffness line  $ab$ . When the voltage is removed at point  $b$  the structure unloads from  $b$  to  $a$  and then along the stiffness line  $ao$ .

The energy method described in Section III can be used to analyse the hybrid actuation scheme by minimising the total potential energy of the two actuator system given by

$$V = \frac{1}{2} \int_0^L EI \left( \frac{d^2 w}{dx^2} \right)^2 dx - [F_1 \sin(\Phi_1) + F_2 \sin(\Phi_2)] \alpha - [F_1 \cos(\Phi_1) + F_2 \cos(\Phi_2)] \varepsilon . \quad (22)$$

where  $F_1$ ,  $\Phi_1$  are respectively the force and the inclination of the piezo actuator in the actuation regime 1 (see Fig. 8 and Fig. 2),  $F_2$  and  $\Phi_2$  denote the force and orientation of the hydraulic actuator in actuation regime 2 (Fig. 8).

Assuming a suitable trial function for the displacement  $w(x)$  parameterised by  $\alpha$  as before in Eqn. (11) and minimising the total potential energy of the system in Eqn. (22) gives the following closed-form approximate expressions:

$$\frac{\alpha}{L} = \frac{8 \left[ \frac{F_1}{P_E} \sin(\Phi_1) + \frac{F_2}{P_E} \sin(\Phi_2) \right]}{\pi^2 \left[ 1 - \frac{F_1}{P_E} \cos(\Phi_1) - \frac{F_2}{P_E} \cos(\Phi_2) \right]} \quad (23)$$

and

$$\frac{\varepsilon}{L} = \frac{\left[ 2 \left[ \frac{F_1}{P_E} \sin(\Phi_1) + \frac{F_2}{P_E} \sin(\Phi_2) \right] \right]^2}{\pi \left[ 1 - \frac{F_1}{P_E} \cos(\Phi_1) - \frac{F_2}{P_E} \cos(\Phi_2) \right]} = \frac{\pi^2 \left[ \frac{\alpha}{L} \right]^2}{16} . \quad (24)$$

Note that  $F_2 = 0$  and  $F_1$  varies from zero to a desired value in the actuation Regime 1 (see Fig. 8). In the actuation Regime 2,  $F_1$  is constant while  $F_2$  varies inducing large displacements  $\alpha$ . The net displacement  $\delta$  along the actuator can be calculated from  $\alpha$  and  $\varepsilon$  according to Eqn. (9).

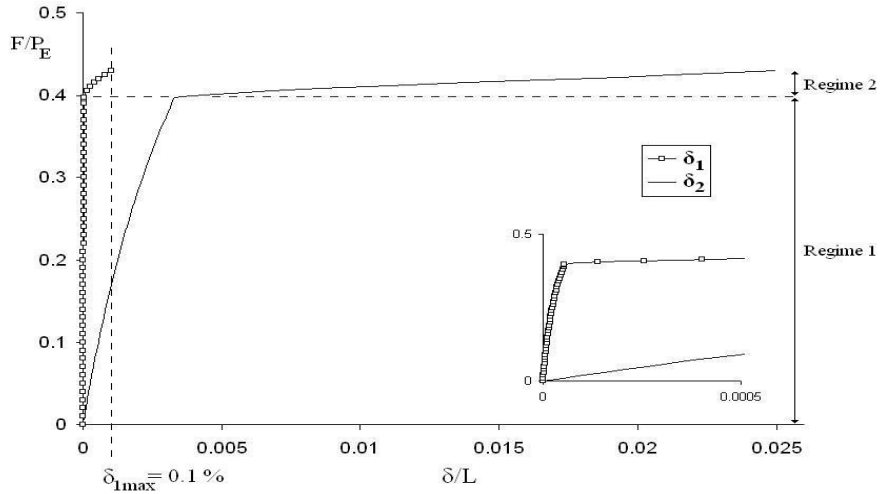


**Figure 9. Example of hybrid actuation. Total actuator force  $F$ , normalized with respect to Euler load  $\pi^2 EI/L^2$ , against displacements, normalized with respect to member length  $L$ , for sway member shown in Fig. 2. The net displacements  $\delta_1$  (squares) and  $\delta_2$  (solids) along the two actuators are shown as a function of the load. The inset in the diagram shows a magnified view for small  $\delta/L$ .**

Hybrid actuation of the strut considered in Section III is illustrated in Fig. 9 by combining a low  $\Phi$  ( $0.5^\circ$ ), large force piezo actuator with a high  $\Phi$  ( $45^\circ$ ), large displacement hydraulic actuator. The strut was loaded to 40% of its Euler load ( $F_1$ ) using the piezo actuator (Regime 1), whereupon the hydraulic actuator induces large displacements, by applying the subsequently small force,  $F_2$  (Regime 2). During Regime 1, the hydraulic actuator tracks the movement induced by the piezo actuator but applies no force, whereas during Regime 2 the piezo actuator maintains a constant force in the strut; following path  $ab$  in Fig. 7, whilst the hydraulic actuator applies force. The displacement along the piezo actuator has to remain small following the switch over<sup>12</sup>. Typically for  $\delta_1/L = 0.1\%$ , the maximum achievable sway is  $\alpha_{\max}/L = 3.4\%$  for this piezo actuator inclination angle. The member always deforms along a set geometric path, but the variation of actuation angle and inclusion of hybrid actuation can alter the force required to perform this deformation. For example, by using purely a piezo actuator ( $\Phi = 0.5^\circ$ ), 83% of the buckling load is required to achieve the maximum allowable deflection ( $\delta_1/L = 0.1\%$  and subsequently  $\alpha/L = 3.4\%$ ). Alternatively, by initially applying 40% of buckling load by piezo actuator ( $\Phi_1 = 0.5^\circ$ ) and then switching to a hydraulic actuator ( $\Phi_2 = 45^\circ$ ), only an additional 3% of buckling load is required. The total force requirement is therefore only 43% of buckling load.

The fact that there is now only a small force requirement on the hydraulic actuator potentially provides controllability benefits. However, practical implementation is likely to require a control algorithm to govern the voltage supplied to the piezo actuator. This needs to be addressed in future studies. The hybrid actuation scheme would be statically indeterminate, improving the stiffness, which would be beneficial if the structure was subjected to aerodynamic loads.

## VI. Conclusions

Analysis of structural morphing of single and multi-element structural assemblies was performed using two techniques: the exact element theory based on stability functions, and an approximate energy method based on an assumed trial function for the displacements. Both these approaches give closed-form relationships between the actuator force and structural displacements. The energy approach, though approximate, was found to be sufficient. Both approaches suggest that larger values of the actuator inclination  $\Phi$  are preferred in the regime of low actuator force. The interaction between the structure and the actuator is modelled using a lumped-parameter approach. The nonlinearity enters the analysis via the structural stiffness. A hybrid actuation scheme to achieve large displacements and forces was introduced and analysed using the energy method to deduce closed-form relationships. The scheme provides scope for optimisation and can potentially improve controllability and stiffness. The closed-form relationships can be readily used in optimisation routines to achieve an optimal structure to produce structural shape changes. Experiments are in progress to verify the analysis presented in this paper.

## Acknowledgments

SP would like to thank the University of Bath for the award of a University Research Fellowship. The authors would like to acknowledge technical discussions with Prof. G. W. Hunt on energy methods.

## References

- <sup>1</sup>Ramrakhyani, D., Lesieutre, G.A., Frecker, M., and Bharti, S., *Aircraft Structural Morphing Using Tendon Actuated Compliant Cellular Trusses*, Journal of Aircraft, Vol. 42 No. 6, Nov-Dec 2005, pp. 1615-1621.
- <sup>2</sup>Seffan, K.A., *Bi-stable concepts for reconfigurable structures*, 45th AIAA/ASME/ASCE/AHS/ASC Structures, Structural Dynamics, and Materials Conference, Palm Springs, California (2004).
- <sup>3</sup>Schultz, M.R., and Hyer, M.W., *A morphing concept based on unsymmetric composite laminates and Piezoceramic MFC actuators*, 45th AIAA/ASME/ASCE/AHS/ASC Structures, Structural Dynamics, and Materials Conference, Palm Springs, California (2004).
- <sup>4</sup>Vos, R. Barrett, R., de Breuker, R., and Tiso, P., *Post-buckled precompressed elements: a new class of control actuators for morphing wing UAVs*, Smart Mater. Struct. Vol. 16, 2007, pp. 919-926.
- <sup>5</sup>Ursache, N.M., Keane, A.J., and Bresslove, N.W., *Design of post-buckled spinal structures for airfoil camber and shape control*, AIAA Journal, Vol. 44, No. 12, Dec 2006, pp. 3115-3124.
- <sup>6</sup>Williams, P.A., Butler, R., Kim, H.A., and Hunt, G.W., *Complementary post-buckling analyses of truss-lattice shear panels*, 48th AIAA/ASME/ASCE/AHS/ASC Structures, Structural Dynamics & Materials Conference, Honolulu, Hawaii, Paper no. AIAA-2007-2124 (April 2007).
- <sup>7</sup>Livesly, R.K. and Chandler, D.B., *Stability functions for structural frameworks*, Manchester University Press, 1956.
- <sup>8</sup>Calladine, C. R., *Buckminster Fuller's "Tensegrity" structures and Clerk Maxwell's rules for the construction of stiff frames*, International Journal of Solids and Structures, Vol. 14, 1978, pp. 161-172.
- <sup>9</sup>Pellegrino, S. and Calladine, C. R., *Matrix analysis of statically and kinematically indeterminate frameworks*, International Journal of Solids and Structures, Vol. 4, No. 2, 1986, pp. 409-428.
- <sup>10</sup>Guest, S. D. and Hutchinson, J. W., *On the determinacy of repetitive structures*, Journal of Mechanic and Physics of Solids, Vol. 51, No. 3, 2003, pp. 383-391.
- <sup>11</sup>Cain, M. and Stewart, M., *The measurement of blocking force*, NPL report MATC (A) 48, National Physical Laboratory, Hampton Road, Teddington, TW11 0LW United Kingdom, September 2001. ISSN: 1473 2734.
- <sup>12</sup>de Vries, J.W.C., *Functional behaviour of multilayer actuators with inactive parts*, Sensors and Actuators A, Vol. 72, 1999, pp. 251-255.
- <sup>13</sup>Hall, D., *Nonlinearity in Piezoelectric ceramics*, Journal of Materials Science, Vol. 36, 2001, pp. 4575-4601.